Modelling of melt on spinning wheels and the impact of scale-up on the various parameters

Problem presented by

Gary Jubb

Thermal Ceramics

Problem statement

Thermal Ceramics manufacture high-temperature thermal insulation, much of which is made in the form of fibre, for use in furnaces, aeroengines, domestic appliances, fire protection systems and other applications. In the manufacturing process, a melt stream emerges from a circular orifice and falls on to two successive spinning wheels, resulting in fiberisation. However, the process also results in a significant fraction of unfiberised material in the form of shot particles. The presence of shot tends to increase the thermal conductivity of the final product. Moreover, some areas of application, such as the automotive industry, require clean fibre with zero shot. Reducing the amount of shot that is produced in the fiberisation process would also reduce the costs of 'cleaning' the fibres for these markets. The Study Group was asked to look at how melt transfers on to the spinning wheels, what kind of melt layer exists on the wheels, and how this layer breaks up. By using a mathematical model to understand the relative importance of various parameters, it is hoped to guide experimental trials and then the scale-up to production levels.

Report prepared by

Chris Breward (University of Oxford)
Rosemary Dyson (University of Oxford)
Carina Edwards (University of Oxford)
Paul Metcalfe (University of Cambridge)
Colin Please (University of Southampton)
Maxim Zyskin (University of Bristol)

Study Group contributors

Chris Breward (University of Oxford)
John Byatt-Smith (University of Edinburgh)
Linda Cummings (University of Nottingham)
Rosemary Dyson (University of Oxford)
Carina Edwards (University of Oxford)
Alistair Fitt (University of Southampton)
Ian Griffiths (University of Oxford)
John Hinch (University of Cambridge)
Peter Howell (University of Oxford)
Sam Howison (University of Oxford)
Gareth Jones (University of Oxford)
Paul Metcalfe (University of Cambridge)
Shailesh Naire (Heriot-Watt University)
Hilary Ockendon (University of Oxford)
John Ockendon (University of Oxford)
Howell Peregrine (University of Bristol)
Colin Please (University of Southampton)
Chris Poole (University of Oxford)
Giles Richardson (University of Nottingham)
Steven Roper (University of Cambridge)
Jennifer Siggers (University of Nottingham)
Frank Smith (University College London)
Jean-Marc Vanden-Broeck (University of East Anglia)
Jennifer Wright (University of Bath)
Xu Xu (Aberdeen University)
Maxim Zyskin (University of Bristol)

1 Introduction[1]

Thermal Ceramics is part of Morgan Crucible plc, and manufactures high temperature thermal insulation, to operate at temperatures in the range 500°C–1600°C. The insulating materials can be in the form of bricks, castables or fibres, of which fibres are the largest and highest growth business. Thermal Ceramics are the equal world number one in the production of high temperature fibrous insulation. Fibre insulation is used in furnaces, aeroengines, domestic appliances, fire protection systems and other applications. The fibre may be used as blanket, board, bulk materials, shaped pieces, paper for seals and so on. Its advantages are the low thermal conductivity (0.05–0.4 W/mK over the range 200°C–1400°C), the low thermal mass (50–300 kg/m^3) and the relatively low cost (£ 2/kg).

[1]This section combines the problem description circulated before the Study Group with the presentation made on the opening day.

In production, the melt is held at a temperature of 1650°C–1950°C, dependent on its chemistry, and has a dynamic viscosity of 1–10 poise at this temperature.

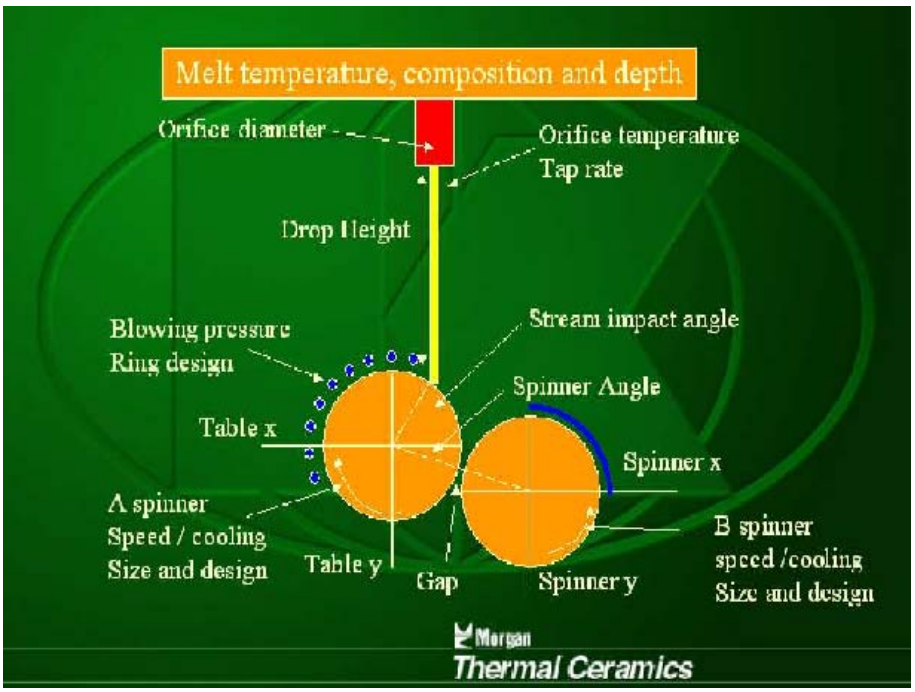

Figure 1: Diagram of fiberisation process

The melt stream emerges from a circular orifice of diameter 5–15 mm, at a tap rate which may be up to 500 kg/hour, falls about 2.5 m, and is fiberised by successive impacts on 2 contrarotating water-cooled steel spinning wheels with parallel horizontal axes as shown in Figure 1, or enlarged in Figure 2. The wheels may be of various diameters; smaller wheels can be spun faster. Generally higher tap rates require larger diameter wheels. It is found that approximately $\frac{1}{3}$ of the fiberisation occurs on the first wheel and $\frac{2}{3}$ on the second. After the second wheel, the material has cooled so far that adding a further wheel would not produce more fiberisation. The gap between the wheels may be 3–10 mm. The main activity occurs in the vertical plane through the orifice perpendicular to the wheel axes. The fibres are blown away from this plane by air from a ring of blowers or a slot (as illustrated on wheels A and B in the figures) producing an air flow parallel to the wheel axes. Among the main parameters are:

- melt temperature, composition and depth,
- orifice diameter,
- orifice temperature,
- tap rate,
- drop height,
- melt stream impact angle,

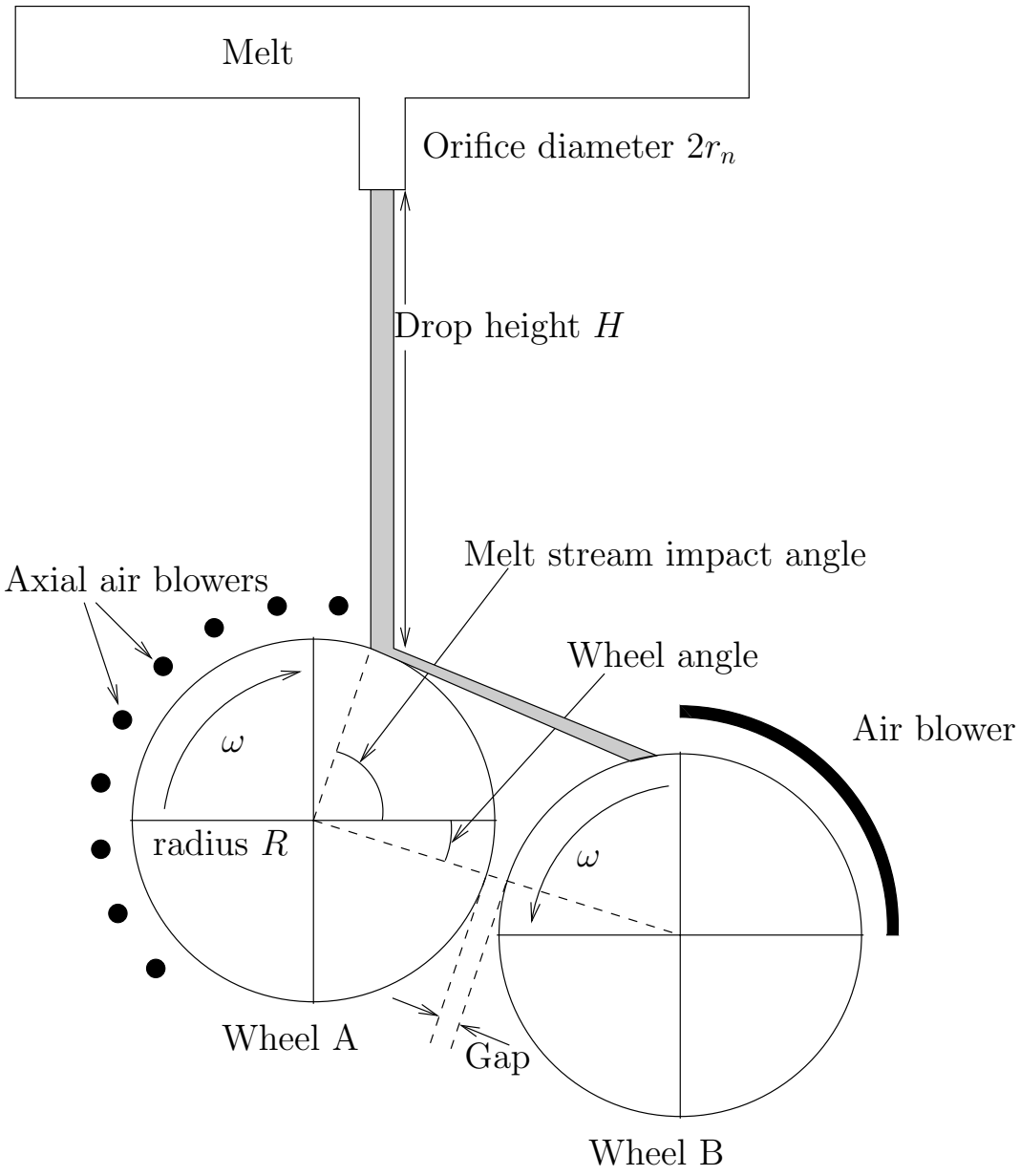

Figure 2: Diagram of wheel operation.

- wheel A diameter, speed and cooling,
- wheel angle,
- wheel B diameter, speed and cooling,
- gap,
- air pressure and ring design.

The viscosity of the melt as a function of temperature is different from that of an ordinary glass, and is roughly as illustrated in Figure 3.

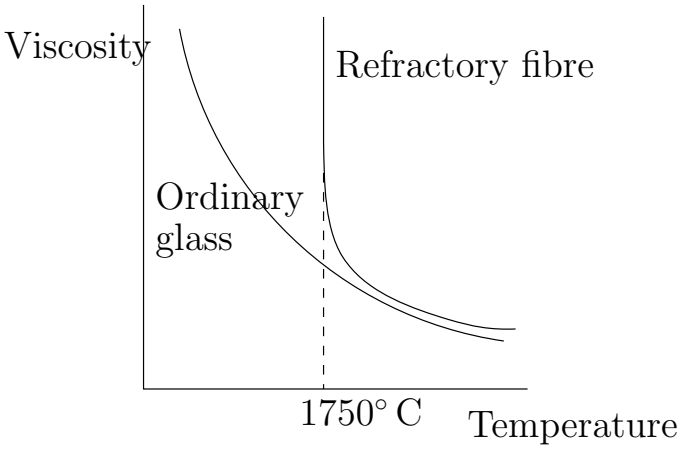

Figure 3: Rough illustration of the contrast between the viscosity-temperature curves for refractory fibre and ordinary glass.

The product from the process consists of the fibres that are the desired output, and also unfiberised material, mainly shot particles, as illustrated in Figure 4.

The fibre diameters are typically between 0.1 and 10 μm, with a log-normal distribution and a mean of 2–3 μm. Generally the unfiberised material is in the form of small spherical beads of glass which the industry refers to as shot. Shot particle diameters can be anything from a few microns to over 1000 μm but are typically between 40–500 μm, with the largest contribution coming from the range 100–250 μm. In practice Thermal Ceramics find that there are few shot particles below 44 μm in diameter, and therefore measure (by sieving) the mass fraction of the product consisting of non-fibrous material with diameter over 44 μm, and define that to be the shot content. In production the shot content is typically in the range 45–55%, which is higher than occurs for normal glasses. The majority of the shot particle diameters fall in the range 75–250 μm and this forms up to 75% of the shot weight.

Figure 4: Scanning electron micrographs of fibres and shot (top), and mainly shot (bottom).

1.1 Importance of shot

Thermal Ceramics would like to reduce the shot content, because it is detrimental to the product in two major areas:

(1) Shot increases thermal conductivity. If it were not there, the thermal conductivity would at worst remain the same, but empirical data suggests that removing shot reduces thermal conductivity. Fibre is generally sold as a needled blanket with densities of the order of 100 kg/m^3. Less material could therefore be sold for the same insulating effect making costs lower and the price lower. One of the big advantages of using fibre over bricks is the saving on thermal mass and therefore any reduction in density will enable savings to be made by customers in their applications.

(2) A growing area of fibre use is in the automotive industry, which requires clean fibre with zero shot. Costs can therefore be improved if the initial shot can be

reduced. This maximises production of fibre for cleaning and will reduce the need for investment in new expensive cleaning equipment as the market increases.

Work has been carried out on reducing shot content on-and-off for 25 years. Shot contents below 45% were achieved on a small scale in the mid-1990s at Thermal Ceramics in the USA, but this cannot be achieved in a controlled or sustainable way, let alone in production. Attempts to move to larger tap rates and larger diameter wheels resulted in shot contents reverting back to over 45%.

1.2 Experiments and modelling work

There is now a development line at Thermal Ceramics to try to improve control of shot content. This has enabled shot content to be reduced, repeating the earlier findings, and demonstrating that it is possible to reduce shot significantly in the process at low tap-rates.

Thermal Ceramics need to explore how the melt transfers onto the wheels, what kind of melt layer exists on them, and how this breaks up into droplets which are flung off to become fibres. Then it will be possible to try to understand what happens as the wheels are increased in size and the melt tap rate is increased, moving towards production scale. The experiments are expensive and time consuming particularly at larger scales, and there are problems associated with running trials in such an environment. In view of this, and the problems with scale-up in the past, it is hoped that a mathematical model will show what parameters are important, whether there is a gradual decrease in effectiveness or a watershed, and so will help to reduce development time and understand potential problems early.

The key points and questions that would help Thermal Ceramics are:

(1) to understand the spray from A onto B;

(2) to explore the melt film stability/instability on the wheels;

(3) to assess how the wheel speed and diameter influence the melt film;

(4) Is there is an optimum melt tap rate for each wheel size ?

(5) Is there is an optimum condition for fibre initiation sites on the wheels ?

2 Approach and notation

We shall approach the problem by studying each stage of the process in turn: the falling melt stream from the furnace to wheel A, the impact on wheel A, the instability of the fluid layer on wheel A, the spray to wheel B, the instability on wheel B, and the fibre dynamics and cooling. We shall use a common set of notation and parameter values, which are listed here. Further notation specific to each part of the study will be introduced in each particular section.

2.1 Values of known quantities

$$
\begin{aligned}
\rho &= \text{melt density } = 2.5 \times 10^3\,\mathrm{kg\,m^{-3}} \\
\gamma &= \text{surface tension } = 0.5\,\mathrm{N\,m^{-1}} \\
T_a &= \text{ambient temperature } = 300\,\mathrm{K} \\
T_m &= \text{temperature of melt } = 2200\,\mathrm{K} \\
c_p &= \text{specific heat of melt } = 10^3\,\mathrm{J\,kg^{-1}\,K^{-1}} \\
k &= \text{thermal conductivity of melt } = 6\,\mathrm{W\,m^{-1}\,K^{-1}} \\
a &= \text{radius of fibre } = 10^{-6}\,\mathrm{m} \\
a_b &= \text{radius of blob } = 1 \times 10^{-4}\,\mathrm{m} \\
\mu &= \text{dynamic viscosity of melt } = 0.1\text{–}1\,\mathrm{Pa\,s} \quad (i.e.\ 1\text{–}10\,\mathrm{poise}) \\
Q_m &= \text{mass flux } = 0.07\,\mathrm{kg\,s^{-1}} \quad (i.e.\ 250\,\mathrm{kg\ per\ hour}) \\
Q_v &= \text{volumetric flux } = 3 \times 10^{-5}\,\mathrm{m^3\,s^{-1}} \\
\kappa &= 2 \times 10^{-6}\,\mathrm{m^2\,s^{-1}} \\
\sigma &= 6 \times 10^{-8}\,\mathrm{W\,m^{-2}\,K^{-4}} \\
H &= \text{fall height } = 2.5\,\mathrm{m} \\
r_n &= \text{nozzle radius } = 3\,\mathrm{mm}
\end{aligned}
$$

The viscosity is assumed to be $\mu = 0.1\,\mathrm{Pa\,s}$ unless stated otherwise.

2.2 Derived quantities

$$
\begin{aligned}
v_n &= \text{speed of melt at nozzle } = 1\,\mathrm{m\,s^{-1}} \\
v_j &= \text{speed of melt at wheel A } = 7\,\mathrm{m\,s^{-1}} \\
r_j &= \text{radius of jet at wheel A } = 1\,\mathrm{mm} \\
H_s &= \text{stable fall height} \\
\omega R &= 100\,\mathrm{m\,s^{-1}} \\
\nu &= \text{kinematic viscosity } = \mu/\rho = 4 \times 10^{-5}\,\mathrm{m^2\,s^{-1}} \\
\delta(x) &= \sqrt{\nu x/(\omega R)} \\
\frac{x}{R} &= 0.02 \\
W_B &= \text{width of melt strip on wheel B } = \tfrac{1}{5}R \\
h &= \text{coating thickness on wheel B } = 2 \times 10^{-5}\,\mathrm{m} \\
\lambda_{\max} &= 3 \times 10^{-4}\,\mathrm{m} \\
\lambda_{\max}^2 h &= 1.8 \times 10^{-12}\,\mathrm{m^3} \\
\beta_{\max} &= \text{maximum growth rate } = 400\,\mathrm{s^{-1}} \quad (\text{using } \mu = 0.1\,\mathrm{Pa\,s})
\end{aligned}
$$

3 From the furnace to wheel A

A thread of molten ceramic leaves the furnace through a nozzle of radius $r_n = 3\,\mathrm{mm}$. The mass flux leaving the furnace is $Q_m = 250\,\mathrm{kg\,hr^{-1}} = 0.07\,\mathrm{kg\,s^{-1}}$, and the fluid density is $\rho = 2.5 \times 10^3\,\mathrm{kg\,m^{-3}}$, so the volume flux leaving the furnace is $Q_v = 3 \times 10^{-5}\,\mathrm{m^3\,s^{-1}}$. Assuming a uniform velocity profile, the speed of the thread on leaving the nozzle is $v_n = Q_v/(\pi r_n^2) \approx 1\,\mathrm{m\,s^{-1}}$.

This thread falls a distance of $H = 2.5\,\mathrm{m}$; by applying Bernoulli's theorem (neglecting viscosity) to the surface streamline we see that the fluid in the thread accelerates to a speed of $v_j = \sqrt{v_n^2 + 2gH} \approx 7\,\mathrm{m\,s^{-1}}$ in falling this distance. To conserve mass the thread must thin; its radius r_j at wheel A satisfies $\pi r_j^2 v_j = \pi r_n^2 v_n = Q_v$, so that $r_j \approx 1\,\mathrm{mm}$. The same argument gives the speed and radius of the jet after falling a distance z; for large z we have $v(z) \approx \sqrt{2gz}$, and so $r(z) \approx (Q_v^2/(2\pi^2 gz))^{1/4}$.

In order to avoid uncontrolled splashing from drop impact on wheel A we require the thread to remain coherent. This provides a constraint on the fall height; surface tension will attempt to break the thread into droplets and the thread must hit wheel A before surface tension manages to break the thread. We can obtain a very crude scaling for this pinch off distance by supposing that surface tension is dominant only when the thread radius is small enough compared with the capillary length $(\gamma/(\rho g))^{1/2}$, the scale on which surface tension acts. In fact, suppose the condition is $r < \alpha(\gamma/(\rho g))^{1/2}$. Then to maintain a coherent thread as far as $z = H$, we need

$$H < H_s = \frac{gQ_m^2}{2\pi^2\alpha^4\gamma^2} - \frac{v_n^2}{2g}. \tag{1}$$

If we take $\alpha = \frac{1}{2}$, that would correspond to assuming that the thread remains coherent as long as its diameter exceeds the capillary length. If we assume this in the Thermal Ceramics problem, we find that the critical height H_s calculated in this way is roughly 10 cm. This is considerably less than the drop height used by Thermal Ceramics, but this crude theory is very sensitive to the precise pinchoff condition used, represented by the parameter α. Also of course, the viscosity will reduce v_j below the Bernoulli value assumed here, and this will increase the thread radius at any given fall distance z.

This problem can be analysed in more detail; this long thin thread can be modelled with lubrication theory. The governing equations, which can be derived from an asymptotic analysis of the Navier-Stokes equations governing fluid flow, are

$$(r^2)_t + (vr^2)_z = 0 \tag{2}$$

$$v_t + vv_z = -(\gamma/\rho)(r^{-1})_z + g + 3\nu(v_z r^2)_z/r^2, \tag{3}$$

where $r(z,t)$ is the thread radius and $v(z,t)$ is the thread speed (see Figure 5 for a sketch of the geometry). Note that all thermal effects have been ignored here, but since this is a relatively thick thread this approximation is reasonable. Scaling the radius r and vertical distance z on the capillary length $(\gamma/(\rho g))^{1/2}$, scaling time t on $(\gamma/\rho)^{1/4} g^{-3/4}$

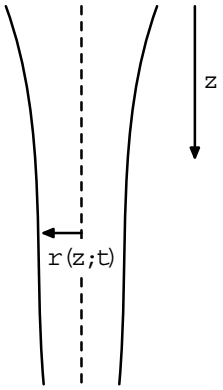

Figure 5: Sketch of geometry of falling thread

and scaling the speed v on $(\gamma/(\rho g))^{1/2}(\gamma/\rho)^{-1/4}g^{3/4}$ we derive the dimensionless set of equations

$$(r^2)_t + (vr^2)_z = 0, \tag{4}$$

$$v_t + vv_z = -(r^{-1})_z + 1 + \epsilon(v_z r^2)_z/r^2, \tag{5}$$

where $\epsilon = 3\nu g^{1/4}(\gamma/\rho)^{-3/4}$. In the Thermal Ceramics problem we find $\epsilon \approx 0.13$, $r(z = 0, t) \approx 0.66$ and $v(z = 0, t) \approx 4.75$. A more detailed study of the breakup of the falling thread would require the numerical solution of these equations, but would provide the dimensionless constant α used in the prediction of the critical fall height H_s.

3.1 Comments

The processes here are amenable to both analytic and experimental study. The extensional flow equations (4) and (5) provide the basis for a numerical investigation, and an asymptotic analysis would also be possible. The high temperatures of the molten ceramic are irrelevant to the physical mechanisms involved in the falling thread problem, and accurate experiments, with safe fluids, seem very possible.

4 On wheel A

The purpose of wheel A seems to be to break the coherent thread of feed into droplets and to throw these droplets onto wheel B in a controlled manner. The relatively slow moving thread of feed lands on wheel A and spreads out in a layer. Viscous forces then accelerate the fluid in this spreading layer up to the wheel speed. This flow is at high Reynolds number — the Reynolds number based on thread thickness and wheel speed is $Re = \omega R r_j/\nu \approx 3000$ — and is governed by the growth of a viscous boundary layer into the nearly stationary fluid that lands on the wheel. As soon as inertial effects are significant, or as soon as the fluid is accelerated to the wheel speed, the layer is thrown off wheel A as a sheet. This sheet breaks up in flight, and impacts on wheel B as droplets.

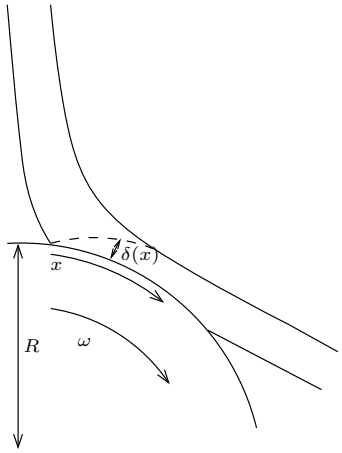

Figure 6: Sketch of geometry of accelerating layer on wheel A

To ensure that the sheet thrown off hits wheel B, it is necessary for the fluid layer to be flung off wheel A very quickly. This condition provides a constraint on the system which we study in this section.

The idea is that the fluid is accelerated by means of a viscous boundary layer that spreads out from the wheel surface. After the fluid has travelled a circumferential distance x on wheel A the thickness of this boundary layer is approximately $\delta(x) = \sqrt{\nu x/(\omega R)}$. When the fluid layer is fully accelerated the mass flux in this boundary layer matches that in the thread, so that

$$Q_v = W_A \delta(x) \omega R, \tag{6}$$

where W_A is the width of the layer on wheel A. This gives a value for the circumferential distance at which the fluid layer is fully accelerated:

$$\frac{x_c}{R} = \frac{Q_v^2}{W^2 R^2 \omega \nu}. \tag{7}$$

Note that it is necessary to predict the width W_A of the fluid layer; an estimated value used during the week of the Study Group was $W_A \approx 3r_j$. A more sophisticated argument given in Section 4.2 predicts $W_A \approx 3.6r_j$ in this problem.

4.1 Some crude experiments in the car park

A number of crude experiments were performed to test this theory using water and shampoo as test fluids. When water was used (shown on the left) the layer did not come off as a sheet — a fine mist of spray appeared around the whole wheel. The shampoo layer (shown on the right) was quickly thrown off the wheel, as desired in the Thermal Ceramics problem. Both experiments had estimated values of $r_j \approx 1\,\mathrm{mm}$, $v_j \approx 1\,\mathrm{m\,s^{-1}}$, $\omega \approx 300\,\mathrm{rad\,s^{-1}}$, and $R \approx 60\,\mathrm{mm}$, with $\nu \approx 10^{-6}\,\mathrm{m^2\,s^{-1}}$ for water and $\nu \approx 10^{-2}\,\mathrm{m^2\,s^{-1}}$ for the shampoo.


Supposing that the layer on the cylinder spreads to a width $W_A = 3r_j$, we find that

$$\frac{x_c}{R} = \frac{Q_v^2}{9r_j^2R^2\omega\nu} = \frac{\pi^2 v_j^2 r_j^2}{9R^2\omega\nu} \ . \tag{8}$$

For the water experiment we find $x_c/R \approx 1$ and for the shampoo experiment we find $x_c/R \approx 10^{-4}$, so that the findings of our experiments are in qualitative agreement with this theory. For the molten ceramic we find that $x_c/R \approx 0.25$, so that the molten ceramic thus occupies an intermediate range between well-behaved shampoo and poorly-behaved water. In terms of operational parameters, we see that (if $W_A = 3r_j$)

$$\frac{x_c}{R} \approx \frac{\pi Q_v\sqrt{2gH}}{9\omega R^2\nu}, \tag{9}$$

so that careful control of the wheel radius R, volume flux Q_v, and fall height H is needed to avoid moving into a regime in which very little ceramic is thrown onto wheel B. A great deal of shot would be produced if the sheet thrown from wheel A failed to hit wheel B.

4.2 Details of thread impact

The boundary layer analysis can be pushed a little further to understand more of the details of the thread impact. We consider the steady flow of a circular thread with volume flux Q travelling at speed V that impacts a flat surface at right angles and where the surface is moving tangentially at speed U. To convert the results here to our wheel problem, note that in the Thermal Ceramics problem $Q = Q_v$, $V = v_j$ and $U = \omega R$. In this section we solve the general problem.

Diagrams of the problem considered are given in Figures 7 and 8, which are a plan view and a side view respectively. We consider a coordinate system with z up the thread, y pointing upstream on the moving surface from the thread impact point and x measuring distance sideways across the moving surface from the thread centreline. We use r as the radial coordinate on the moving surface. The curve where the fluid depth goes to zero

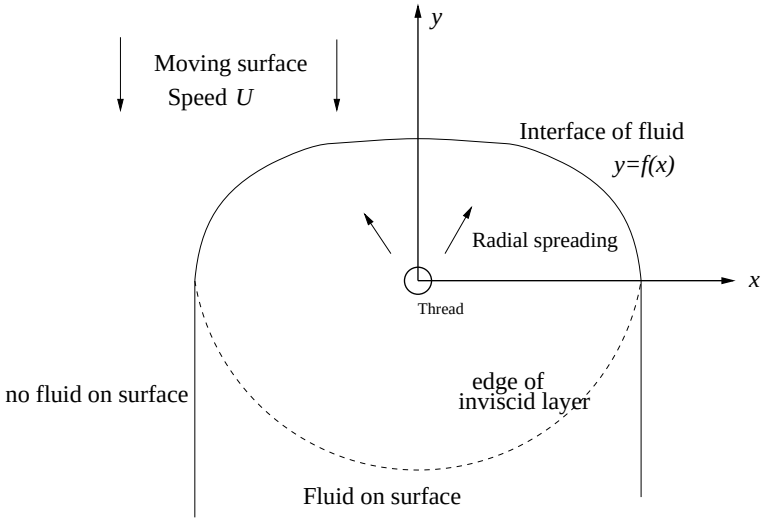

Figure 7: A top view of the cylindrical thread impinging on the moving surface

and there is no fluid remaining on the surface is taken to be $y = f(x)$. This curve is a free boundary which needs to be found. It also gives the position of the start of the viscous boundary layer. Note that there is another curve (where $y < 0$ and shown with the dotted curve in the figure) where the depth of the inviscid layer goes to zero but the boundary layer is of finite thickness. Beyond this curve the fluid basically moves with the velocity of the surface. We shall not consider this second curve in detail in this section; a scaling for the important features of this curve is given in (7).

In the inviscid layer we note that the radial velocity is a constant V by Bernoulli. Conservation of mass implies that $2\pi hrV \to Q$ as $r \to 0$, and that

$$\frac{1}{r}\frac{\partial}{\partial r}\left(rhV\right) = v_{BL}, \tag{10}$$

where v_{BL} is the vertical velocity of fluid drawn into the thin boundary layer.

In the viscous boundary layer we consider the boundary layer equations

$$\frac{\partial u}{\partial y} + \frac{\partial v}{\partial z} = 0, \tag{11}$$

$$u\frac{\partial u}{\partial y} + v\frac{\partial u}{\partial z} = \nu\frac{\partial^2 u}{\partial z^2}, \tag{12}$$

where u is the component of velocity in the y direction and v is the component of velocity in the z direction. The boundary conditions are that $u = -U$ and $v = 0$ on the moving surface $z = 0$. In addition we require that $u \to 0$ as $z \to \infty$ since we are considering the case $V \ll U$ in which the inviscid layer appears nearly stationary to the viscous

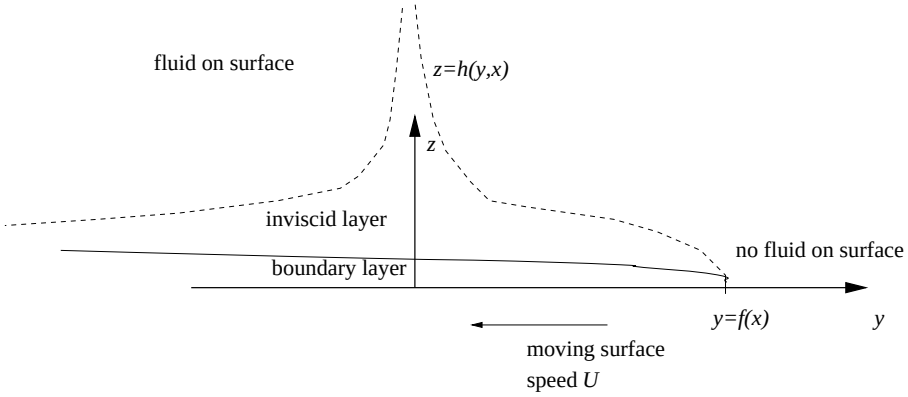

Figure 8: A side view of the cylindrical thread impinging on the moving surface

boundary layer. Note that we have neglected any possible crossflow in the boundary layer; this is justified by supposing that the flow is much wider than it is thick. Finally, we suppose that the boundary layer starts on the curve $y = f(x)$, at which the inviscid layer has its maximal upstream extent.

We first aim to determine the flow rate into the boundary layer. This is simply given by v_{BL}, which is the limit of v as $z \to \infty$. A standard scaling argument shows that we can find a similarity solution in which

$$v_{BL} = \sqrt{\frac{U\nu}{f(x) - y}}\, G_\infty, \tag{13}$$

where to find G_∞ we need to solve the Blasius equations

$$-\frac{\eta}{2}F' + G' = 0 \tag{14}$$

$$-\eta F F' + G F' = F'' \tag{15}$$

with $F(0) = 1$, $G(0) = 0$ and $F \to 0$ as $\eta \to \infty$, where $\eta = z\sqrt{U/\big(\nu(f(x) - y)\big)}$. From this solution we can determine the value of G_∞ using $G_\infty = \lim_{\eta\to\infty} G(\eta)$. Using standard numerical boundary value software we find that $G_\infty \approx -1.143$; as required there is flow into the boundary layer.

The resulting problem for the inviscid layer can now be put into nondimensional form. We scale the coordinates x, y, r and $f(x)$ with a length L, and we scale height h with $h_0 = Q/(2\pi V L)$. It is then found that by choosing the natural length scale $L = \big(Q^2/(4\pi^2 U\nu G_\infty^2)\big)^{1/3}$ the problem becomes

$$\frac{1}{r}\frac{\partial}{\partial r}(rh) = \frac{-1}{\sqrt{f(x) - y}}\,, \tag{16}$$

with $h \sim 1/r$ as $r \to 0$ and $h = 0$ on $y = f(x)$.

The Reynolds number Vh_0/ν of the inviscid layer will be large if $QU \gg \nu^2$, while $U \gg V$ ensures both that the inviscid layer appears stationary relative to the boundary layer and that the boundary layer thickness is small compared to the inviscid layer thickness ($h_0 \gg \sqrt{L\nu/U}$). Finally we require $L \gg h_0$ in order that the thin layer approximations for the spreading inviscid layer are valid; this requires $QV^3 \gg (U\nu)^2$. All of these conditions are satisfied by the Thermal Ceramics problem.

We can integrate (16) using the boundary condition as $r \to 0$ to get

$$h(r,\theta) = \frac{1}{r}\int_0^r \frac{-q\,\mathrm{d}q}{\sqrt{f(q\cos\theta) - q\sin\theta}} + \frac{1}{r}. \tag{17}$$

We then impose the condition $h = 0$ on the curve $y = f(x)$ by insisting that on the curve $r = \sqrt{x^2 + f(x)^2}$, $\cos\theta = x/r$ and $\sin\theta = f(x)/r$, and hence

$$0 = \int_0^{\sqrt{x^2+f(x)^2}} \frac{-q\,\mathrm{d}q}{\sqrt{f\left(qx/\sqrt{x^2+f(x)^2}\right) - qf(x)/\sqrt{x^2+f(x)^2}}} + 1 \tag{18}$$

Changing the variables in the integral then gives us

$$1 = \left(x^2 + f(x)^2\right)\int_0^1 \frac{q\,\mathrm{d}q}{\sqrt{f(qx) - qf(x)}}\,, \tag{19}$$

a nonlinear integral equation for the function $f(x)$. From this, we can easily find one point on the curve by considering the point of symmetry $x = 0$. In this case the equation reduces to

$$1 = f(0)^2\int_0^1 \frac{q\,\mathrm{d}q}{\sqrt{f(0) - qf(0)}}, \tag{20}$$

where we can readily evaluate the integral and hence find that $f(0) = 6^{2/3}/4 \approx 0.82548$. This then gives an expression for the maximum distance upstream of the thread impact point reached by the fluid layer:

$$\tfrac{1}{4}\,6^{2/3}\left(\frac{Q^2}{4\pi^2 U\nu G_\infty^2}\right)^{1/3}, \tag{21}$$

which in the Thermal Ceramics problem is approximately one thread radius.

Series solutions to the integral equation (19) can be readily computed using MAPLE, giving

$$\begin{aligned} f(x) =& \frac{1}{4}\,6^{2/3} - \frac{5}{18}\,6^{1/3}x^2 - \frac{1}{9}x^4 - \frac{91}{6561}\,6^{2/3}x^6 \\ &- \frac{748}{59049}\,6^{1/3}x^8 - \frac{28}{2187}x^{10} - \frac{9880}{43046721}\,6^{2/3}x^{12} - \ldots. \end{aligned} \tag{22}$$

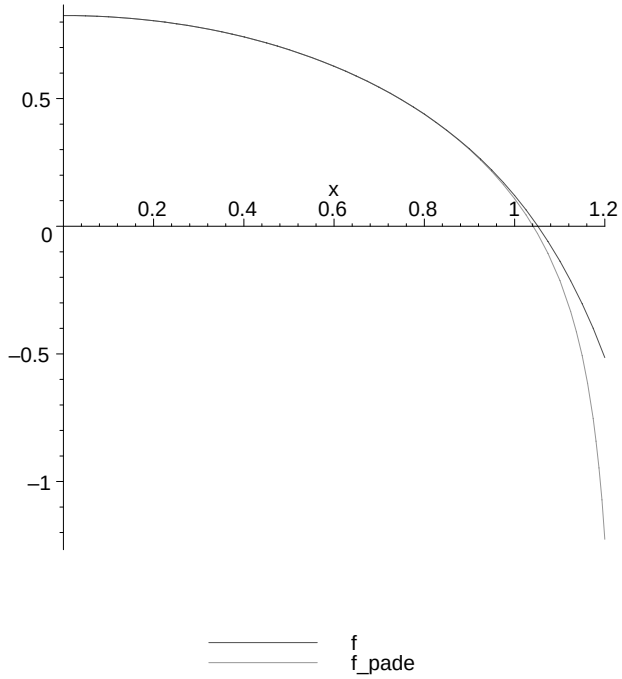

Figure 9: The upstream boundary of the thread impact layer

This 12^{th} order polynomial is plotted in Figure 9, together with its $[6,6]$ Padé approximant. This approximant has simple poles at $x \approx \pm 1.25$, possibly showing that the downstream width of this spreading layer is $2L \times 1.25 = 2.5L$. Assuming that these poles do give the layer width, and bringing back the physical lengthscales, we see that the downstream width of the spreading layer is approximately 3.6 mm, which is roughly 3.6 thread radii. If this approach is used generally, then the parametric dependence of the width W_A of the layer on the wheel is not simply $W_A = 3r_j$ but

$$W_A = 2.5L = 2.5 \left(\frac{Q_v^2}{4\pi^2 \omega R \nu G_\infty^2} \right)^{1/3} . \tag{23}$$

4.3 Comments

The simple theory presented here is relatively crude, and a less crude theory is very difficult. However, this problem is amenable to relatively simple experiments — the high temperatures of the molten ceramic are irrelevant to the processes throwing the fluid layer off wheel A. It is therefore possible to use safer fluids to study this process more accurately; this should be done if more insight into the process is sought.

5 Spray onto wheel B, instability on wheel B

We assume that the melt arrives at wheel B with velocity $\omega R \approx 100\,\text{m/s}$, and in droplets with diameter of order $\delta(x_c)$. The distance travelled from the contact point on wheel

A to the contact point on wheel B is of order R. We expect the angle of spread (in the plane perpendicular to that shown in Figure 2) to be about 10°, since all turbulent spread angles are 10°, so the width of the melt strip on wheel B will be $W_B \approx R/5$. (This agrees with observations by Thermal Ceramics of a strip of width 15 mm in a case where $R = 75\,\mathrm{mm}$.)

The melt arriving on wheel B will then form a layer of thickness h given by

$$h = \frac{Q_v}{W_B \omega R} \approx 2 \times 10^{-5}\,\mathrm{m}. \tag{24}$$

The influence of the angle of impact onto wheel B was not studied, but both this and the assumption mentioned earlier about droplet size could be studied by high speed photography of an equivalent cold experiment.

We now consider the layer of thickness h on wheel B, which will be unstable because of the centrifugal acceleration $\omega^2 R$, but with a stabilizing effect due to surface tension. The combination of these will give a characteristic wavelength of the instability of order

$$\lambda_{\max} = 2\pi\sqrt{\frac{2\gamma}{\rho\omega^2 R}} \approx 3 \times 10^{-4}\,\mathrm{m}, \tag{25}$$

and therefore the "volume of instability" will be of order $V = \lambda_{\max}^2 h \approx 1.8 \times 10^{-12}\,\mathrm{m}^3$: the volume of melt in a square of size $\lambda_{\max}$ of the layer of thickness h. If we assume this either forms a shot particle or a fibre, than as shot, V is the volume of a sphere of radius about $100\,\mu$m, which is about right for the typical large shot particles. If alternatively we write V as the volume of a fibre of diameter $2\,\mu$m, then the fibre length is 56 cm, again of the right order of magnitude. The rate of production of volumes V will be $q_v/V \approx 10^7$ (fibres or shot particles) per second. Note though that these calculations do not say what the shot : fibre proportions will be at all.

A further step is to compute the growth rate of the instability on wheel B. If the layer thickness h is now regarded as a variable $h(x,t)$, then it will obey

$$h_t + \left(\frac{h^3}{3\mu}(\rho\omega^2 R h + \gamma h_{xx})_x\right)_x = 0, \tag{26}$$

and the maximum growth rate $\beta_{\max}$ will be of order

$$\beta_{\max} = \frac{h^3(\rho\omega^2 R)^2}{12\mu\gamma} \approx 400\,\mathrm{s}^{-1}. \tag{27}$$

The time taken for the instability to develop by a factor of order 1 is thus of order $1/\beta_{\max}$. Since the melt arrives on wheel B as droplets, we may assume the surface is initially crinkly—these instabilities do not have to grow from zero—and we may assume that in a time of order $1/\beta_{\max}$ the layer has been flung off completely. Naturally, we wish this to happen *within* one revolution, so we would like to ensure $\omega/\beta_{\max} \leq 2\pi$. In

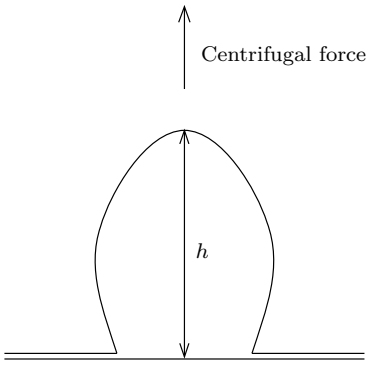

Figure 10: The drop before jet initiation

fact for the representative values we have computed, $\omega/\beta_{\max} \approx 5$ so this condition does hold.

If we now move on to consider the problem of jet initiation—how the shape of a droplet will form during the process of it being flung off from wheel B—the simplest model is to draw an analogy with pendant drops, with gravity being supplied by the centrifugal force. The Laplace-Young equation needs to be integrated numerically as in [2] and a calculation along these lines is included in Appendix A. This reveals that no steady shape with finite radius of curvature could exist if the droplet depth h illustrated in Figure 10 is too large.

Even though no detailed droplet initiation calculation has been carried out, we shall need an estimate of the initiation velocity v_{in} with which material leaves the sheet on wheel B, in order to try to understand the initial stages of fibre dynamics and cooling. This initiation velocity is determined by the balance between the viscous stress of order $\mu v_{\text{in}}/h$ and the inertial stress difference $\rho\omega^2 Rh$ across the layer of thickness h. Equating these shows

$$v_{\text{in}} \sim \rho\omega^2 Rh^2/\mu = \omega^2 Rh^2/\nu \approx 2\,\text{m/s}. \tag{28}$$

6 Fibre and shot dynamics

After the fibre has been ejected from the layer on wheel B, it flies through the air and cools as it goes. In this section we think about the heat transfer processes and formation of fibres and shot. In each calculation, we focus on determining order-of-magnitude estimates, rather than solving models.

We show a schematic of the situation in Figure 11. We are interested in finding an estimate for the radius, a, of the fibre and for the length, L, after which the fibre has solidified. As seen in Section 5, the liquid leaves the wheel at speed $v_{\text{in}} \sim \rho\omega^2 Rh^2/\mu$. Providing the fibre remains liquid for long enough, conservation of mass implies that

$$\frac{\rho\omega^2 Rh^2}{\mu}\pi h^2 = \omega R\pi a^2 \qquad i.e. \qquad a = h^2\sqrt{\frac{\rho\omega}{\mu}} \approx 1\times 10^{-6}\text{m}, \tag{29}$$

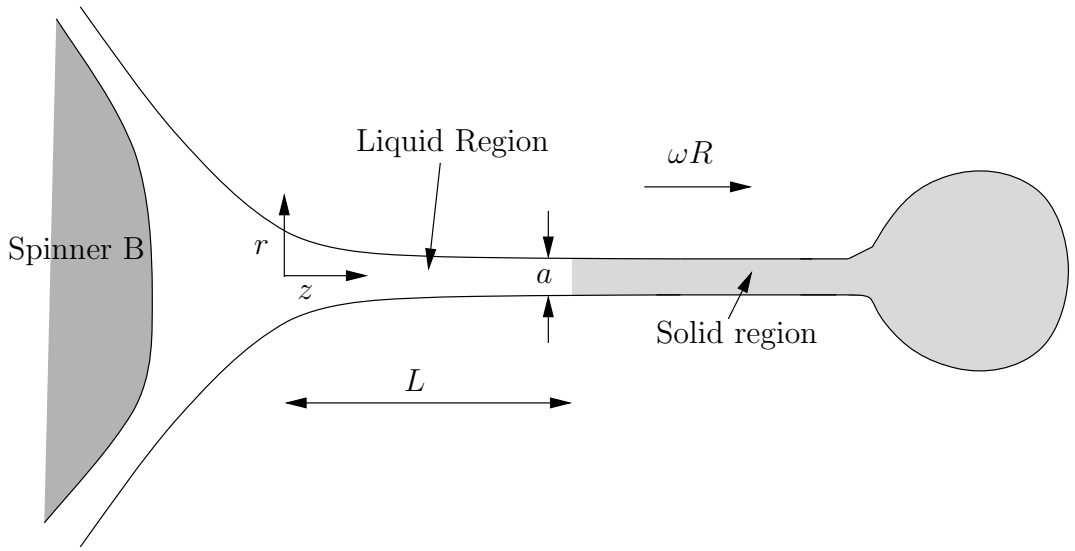

Figure 11: Schematic showing the shot and fibre leaving wheel B

which is consistent with the observed fibre thickness.

A paradigm model for the temperature, T, in the fibre once it has formed is

$$\frac{\rho c_p}{k}\frac{\partial T}{\partial t} = \frac{\partial^2 T}{\partial z^2} + \frac{1}{r}\frac{\partial}{\partial r}\left(r\frac{\partial T}{\partial r}\right), \tag{30}$$

with

$$-k\frac{\partial T}{\partial r} = E\sigma\left(T^4 - T_a^4\right) \qquad \text{on} \qquad r = a, \tag{31}$$

$$\frac{\partial T}{\partial r} = 0 \qquad \text{on} \qquad r = 0, \tag{32}$$

$$T = T_s \qquad \text{at} \qquad z = L, \tag{33}$$

$$T = T_0 \qquad \text{at} \qquad z = 0, \tag{34}$$

where ρ is the density, c_p is the specific heat, k is the heat conductivity, E is the emissivity of the surface, σ is the Stefan-Boltzmann constant, T_a is the air temperature, T_s is the melting temperature and T_0 is the temperature that the fibre leaves the wheel.

We nondimensionalise the system using

$$z = Lz', \qquad r = a_0 r', \qquad t = \tau t', \qquad T = T_f T' \qquad a = a_0 a', \tag{35}$$

where a_0 is a typical fibre radius and T_f is the temperature of the fibre. The nondimensional problem reads

$$Pe\frac{\partial T}{\partial t} = \epsilon^2\frac{\partial^2 T}{\partial z^2} + \frac{1}{r}\frac{\partial}{\partial r}\left(r\frac{\partial T}{\partial r}\right), \tag{36}$$

with

$$-\frac{\partial T}{\partial r} = S\left(T^4 - \bar{T}_a^4\right) \quad \text{on} \quad r = a\,, \qquad\qquad \frac{\partial T}{\partial r} = 0 \quad \text{on} \quad r = 0\,, \tag{37}$$

where $Pe = \rho c_p a_0^2/k\tau$, $\epsilon = a_0/L$, $\bar{T}_a = T_a/T_f$, and $S = E\sigma T_f^3 a_0/k$, where τ is to be determined by balancing forces.

Firstly, we consider the timescale, τ_c, for transverse cooling, namely

$$\tau_c = \frac{\rho c_p a_0^2}{k}. \tag{38}$$

If we assume that fibres have radius 1μm and that shot have radius 0.1mm, the timescales for cross-fibre and sphere cooling are

$$\tau_{c(\text{fibre})} = 4 \times 10^{-7}\text{s}, \qquad \tau_{c(\text{shot})} = 4 \times 10^{-3}\text{s}. \tag{39}$$

As seen in Section 5, the fibres are flung off at a speed of $100\,\mathrm{m\,s^{-1}}$. Thus the distance travelled by the fibre before its temperature is uniform across the fibre is of the order of $50\,\mu$m. Similarly, we calculate that the distance travelled by the shot prior to the temperature being uniform is 50 cm. We conclude that the molten fibre achieves uniform temperature across its section very close to the wheel.

In order to gain an estimate for L, we need to know the sizes of Pe and S. For a 1μm fibre, we calculate that $S \approx 8 \times 10^{-5}$, $Pe \approx 4 \times 10^{-7}/\tau$ and $\epsilon \approx 10^{-6}/L$. We can relate τ and L using $\tau \approx L/U$, where $U \approx 100\,\mathrm{m\,s^{-1}}$ is the velocity that the fluid is flung off, to give that $Pe/\epsilon \approx 40$. Thus we find that we are operating in a regime where $Pe = O(\epsilon)$ and $S = O(\epsilon)$. If we seek a power series expansion for the solution to (36) and (37), we find at leading order that $T = T_0(z,t)$. At the next order in the equations and boundary conditions, we find that

$$\mathcal{P}\frac{\mathrm{d}T_0}{\mathrm{d}t} = \frac{1}{r}\frac{\partial}{\partial r}\left(r\frac{\partial T_1}{\partial r}\right), \tag{40}$$

with

$$-\frac{\partial T_1}{\partial r} = \mathcal{S}\left(T_0^4 - \bar{T}_f^4\right) \quad \text{on} \quad r = a\,, \tag{41}$$

where $\mathcal{P} = Pe/\epsilon$ and $\mathcal{S} = S/\epsilon$. We find that

$$a\frac{\mathrm{d}T_0}{\mathrm{d}t} = -2\frac{\mathcal{S}}{\mathcal{P}}\left(T_0^4 - \bar{T}_f^4\right). \tag{42}$$

Assuming that the temperature drop required to reach solidification is $\Delta T/T_f$ where $\Delta T \approx 400$ K, we can estimate L by setting

$$\frac{\Delta T}{T_f} = 2\frac{\mathcal{S}}{\mathcal{P}}\,, \qquad i.e. \quad \tau = \frac{\rho c_p a_0 \Delta T}{2E\sigma T_f^4} \approx 4 \times 10^{-4}\ \mathrm{s}\,, \tag{43}$$

and so

$$L = U\tau = \frac{\rho c_p a_0 \Delta T U}{2E\sigma T_f^4} \approx 4 \text{ cm}. \tag{44}$$

Thus, the fibre solidifies shortly after it leaves the wheel and the majority of the fibre length is solid as it flies through the air. We can conclude that it is not possible to reduce the volume of the shot during this stage of the process, since the solid fibre is unable to draw any liquid out of the shot.

We note at this stage that, of course, our fibre radius changes as the fibre extends and so our timescales are quite rough. A simulation of the fully coupled fluid flow and mass transfer processes would be required to tie down the timescale more accurately.

Our final concern is whether the fibre will be coherent when it solidifies, or whether a combination of inertial, surface tension and viscous forces can result in fibre rupture before it solidifies. The equations governing the evolution of the fibre are

$$(a^2)_t + \left(a^2 u\right)_z = 0, \tag{45}$$

$$\rho a^2 \left(u_t + u u_z\right) + \gamma a^2 \left(\frac{1}{a} - a_{zz}\right)_z = 3\left(\mu a^2 u_z\right)_z, \tag{46}$$

subject to boundary conditions

$$u = v_{\text{in}} \qquad \text{at} \qquad z = 0, \tag{47}$$

$$u = \omega R \qquad \text{at} \qquad z = L, \tag{48}$$

7 Thermal interaction of the melt with the wheel

The steel wheels on which the melt is deposited must withstand temperatures of up to 2200 K and are thus water cooled. This water cooling creates a layer of solidified melt on the wheel. We now estimate the thickness of this layer, and consider its effect on the spinning process.

We take the solidification temperature of the melt to be 1800 K, and so consider that the melt forms solid and liquid layers on the wheel as illustrated in Figure 12. (The solidification temperature may in fact be somewhat higher than this, but we shall use this figure to illustrate the approach.) The solidified melt occupies a layer of thickness l_{glass}, and the liquid melt a layer of thickness h. The temperature of the surface of the wheel is T_s, and we assume for the present that $T_s \approx 800$ K.

When we apply the hot melt to the wheel the previously solidified material melts and the solidification front $x_s(t)$ retreats from, and subsequently advances back into, the applied liquid melt. If the melt remains on the wheel for too long it will completely solidify. Equally drawing the liquid melt off into the fibres too quickly will take not only the deposited melt, but also some of the remelted solid. If we assume that the system is in equilibrium then the time taken for the instability to develop must balance the time $\hat{t}$

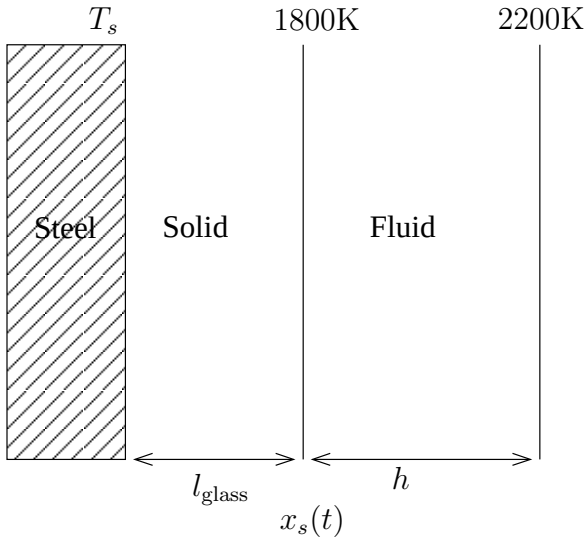

Figure 12: A diagram of the solidification of the melt onto the wheel.

taken for the layer h to cool from 2200 K to 1800 K by conduction through $l_{\rm glass}$, *i.e.* for $x_s(\hat{t}) \approx x_s(0)$. To be in equilibrium we thus require that

$$\hat{t} \;=\; \frac{1}{\beta_{\max}}\,, \tag{49}$$

where $\beta_{\max}$ is given by (27).

To estimate $\hat{t}$ we consider the heat equation

$$\rho c_p \frac{dT}{dt} \;=\; -\frac{d\mathrm{q}}{dx}\,, \tag{50}$$

where ρ is the density, c_p the specific heat, T the temperature, and q is the outward heat flux as given by

$$\mathrm{q} \;=\; -k\frac{dT}{dx}\,. \tag{51}$$

We see from (51) that the heat flux through $l_{\rm glass}$ is $O(1000k/l_{\rm glass})$, and thus the time taken for the fluid layer to cool by 400 K is

$$\hat{t} = \frac{\rho c_p 400 h l_{\rm glass}}{1000k}\,, \tag{52}$$

which may be substituted into (49) to give an estimate for $l_{\rm glass}$. Taking $\rho = 2.5\times10^3\,\mathrm{kg\,m^{-3}}$, $c_p = 10^3\,\mathrm{J\,kg^{-1}\,K^{-1}}$, and $k = 6\,\mathrm{W\,m^{-1}\,K^{-1}}$, with (from Section 5) $h = 2\times10^{-5}\,\mathrm{m}$, and $\beta_{\max} = 400\,\mathrm{s^{-1}}$, we find that

$$l_{\rm glass} = 7.5\times10^{-4}\,\mathrm{m}. \tag{53}$$

This is a very rough estimate for $l_{\rm glass}$ depending on several *ad hoc* assumptions, most notably that the temperature of the wheel surface T_s is equal to 800 K. To improve the estimate we would require further information on the wheel cooling mechanism.

To predict the position of the solidification front $x_s(t)$, and thus l_{glass}, accurately we must solve the heat equation in the wheel, in the solid phase, and in the fluid phase, with appropriate boundary conditions applied at each interface. Suitable boundary conditions would be that there is no heat flux across the liquid melt surface, and that the temperature is continuous across the interfaces between the steel and solidified melt, and between the solidified and liquid melt. Additionally we assume that the temperature at the water cooled surface is fixed by the water temperature. The analysis is greatly complicated as the interface between the solid and liquid phases is an unknown *free boundary* $x_s(t)$. To complete the system and fix the free boundary $x_s(t)$ we must further impose the *Stefan condition* [1], which relates the difference in the temperature gradients on either side of $x_s(t)$ to the latent heat of the melt. The full calculation of the temperature profiles and the position of $x_s(t)$ is thus a non-trivial calculation which requires further physical parameter values.

8 Conclusions

We have studied each stage of the fiberisation process in enough detail to identify the main governing parameters and constraints. These outline models agree with observed values, lead to recommendations for making shot smaller, and suggest some bounds that the operating values should be kept within. In particular the process has been broken down into:

(1) **Jet feed:** Surface tension will always cause the jet to break up into droplets after a certain distance, and we recommend that the drop height should be kept below this distance, because jet break-up will cause splashing and droplet bouncing on wheel A which will tend to produce more shot and less fibre.

(2) **Speed-up on wheel A:** We have studied the acceleration of the melt stream after its contact with wheel A, and we recommend that the distance x over which the layer reaches full speed should be kept below $0.1R$.

(3) **Flow onto wheel B:** We have analysed the spray sheet onto wheel B, obtained an estimate of the coating thickness, and analysed the centrifugally-driven surface instability. This leads to predictions of the maximum shot size and typical fibre size that are in good agreement with the observed values—but it does not predict the shot:fibre ratio. This analysis also suggests ways of making shot smaller, either by reducing the tap rate Q_m, or increasing the linear velocity on the wheel ωR. (Though of course, reducing Q_m reduces the allowable stable drop height H, and there are engineering constraints on wheel speed.)

(4) **Fibre and droplet cooling:** We have considered the cooling process when a droplet and fibre leave the melt layer, and shown that the fibre will be solid by the time it has separated by about 3 cm from the wheel.

(5) We have briefly considered the thermal interaction of the melt with the wheel, and the thickness of the solid glass layer formed. This could be taken further given more information about the construction of the drum.

For the future we have suggested:

(1) **Cold experiments:** These can be easy and informative. In particular, suitable cold experiments could be used to study

- the stable fall distance of the jet;
- the impact of the spray from wheel A onto wheel B (this would need high speed photography of the cold experiment).

(2) **A hot experiment**, perhaps using molten sugar or candlewax, would be useful to study the drawing of a solidifying fibre.

(3) **Shot/fibre ratio:** this is governed by the drawing, cooling and solidification process, and needs further work, possibly through a PhD project.

A Stationary droplet in centrifugal force

With reference to Section 5, we are interested in the shape of a droplet on the surface of a large cylinder of radius R, rotating with constant angular velocity ω, just before the droplet breaks away from the surface, roughly as illustrated in Figure 13. This is

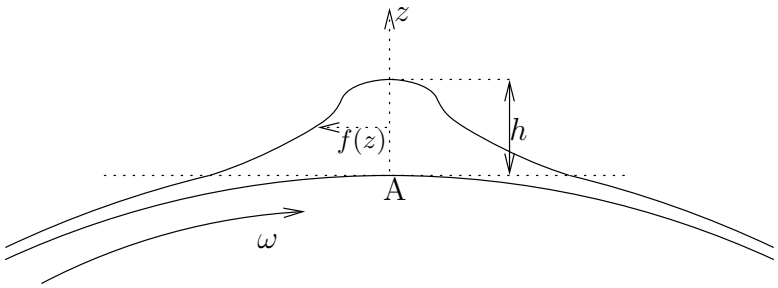

Figure 13: Diagram of liquid droplet in steady rotation on a large cylinder.

essentially the same problem as a droplet falling from a ceiling. While the droplet is stationary, we have the equilibrium equation for the liquid inside the drop, balancing the centrifugal force with the pressure gradient:

$$-\rho\omega^2 r = -\frac{dP}{dr}\,, \quad R < r < R + h\,, \tag{54}$$

where $P(r)$ is pressure, and h is the height of the drop. Let $z = r - R$, so then

$$\frac{d}{dz}P(z) = \rho\omega^2(z + R)$$

and

$$P(z) = p_0 + \rho\omega^2\left(Rz + \frac{z^2}{2}\right). \tag{55}$$

If we assume that there is a thin layer of liquid on the surface of cylinder to which the droplet connects, as in Figure 13, then at the bottom of the droplet ($z = 0$) the pressure is $p_0 = p_a + \gamma/R$, where p_a is atmospheric pressure. We shall see later that this leads to a difficulty, so we keep p_0 general at present.

The jump of pressure across the surface of the droplet is therefore $(p_0 - p_a) + \rho\omega^2 (Rz + z^2/2)$. This jump of pressure must be balanced by surface tension, thus

$$\gamma 2H(z) = (p_0 - p_a) + \rho\omega^2 \left(Rz + \frac{z^2}{2} \right), \quad 0 \le z \le h\,, \tag{56}$$

where $H(z)$ is the mean curvature of the surface of the droplet (that is, $2H = 1/R_1 + 1/R_2$ where R_1 and R_2 are the principal radii of curvature). Thus

$$2H(z) = \frac{p_0 - p_a}{\gamma} + \left(\frac{\rho\omega^2}{\gamma} \right) \left(Rz + \frac{z^2}{2} \right). \tag{57}$$

This implies that the length scale L of the droplet is given by $L^2 = \gamma/(\rho\omega^2 R)$ and for our representative values this gives $L \approx 3 \times 10^{-5}\,\mathrm{m}$, so $L/R \approx 5 \times 10^{-4}$. Therefore when we scale the droplet size with L, the cylinder appears approximately *flat* as far as the droplet is concerned, and so we can then assume that the droplet is axisymmetric about the axis Az in Figure 13.

If the profile of the droplet is given by a function $f(z)$ as in Figure 13, its mean curvature is given by $2H = -f''/(1 + f'^2)^{3/2} + 1/(f\sqrt{1 + f'^2})$. If we rescale all distances with L (so h/L, z/L, R/L are now called h, z, R) then we have

$$\frac{-f''}{(1 + f'^2)^{3/2}} + \frac{1}{f\sqrt{1 + f'^2}} = c + z + \frac{z^2}{2R}\,, \tag{58}$$

where $c = L(p_0 - p_a)/\gamma$. Really, it is inconsistent to retain the last term on the right of this equation, since we are assuming $R \gg 1$: if we wished to work accurately to terms of order $1/R$ then we should assume a general droplet shape (which cannot be axisymmetric about Az) and there would be terms of order $1/R$ in the expression for the curvature that would have to be included. Nevertheless, the term $z^2/(2R)$ has been retained in the calculations presented below.

At the top of the droplet we have $f(h) = 0$. Very close to the top, the surface is approximately a sphere, and thus near the top

$$f(z) \approx \lambda\sqrt{h - z}\,, \quad \lambda(h) = \sqrt{\frac{4R}{Rc + Rh + h^2/2}}\,. \tag{59}$$

Let $s = h - z$, and let $y(s) = f(h - z)$. Then

$$\frac{-y''}{(1+y'^2)^{3/2}} + \frac{1}{y\sqrt{1+y'^2}} = c + (h-s) + \frac{(h-s)^2}{2R}\,, \tag{60}$$

with initial data near the top of the droplet given by

$$y(\epsilon) = \lambda(h)\sqrt{\epsilon}\,, \quad y'(\epsilon) = \lambda(h)\,\frac{1}{2\sqrt{\epsilon}}\,. \tag{61}$$

A solution of (60) and (61) exists up to a certain value $s_{max} > \epsilon$. For the drop of height h to exist, we should have $s_{max} \geq h$. If $s_{max} < h$, there is no solution of this height which ends with a top, which means that either the droplet breaks off, or there is a jet forming. We do not investigate here the jet solution, which is more complicated and will involve finding velocities and pressure of the liquid.

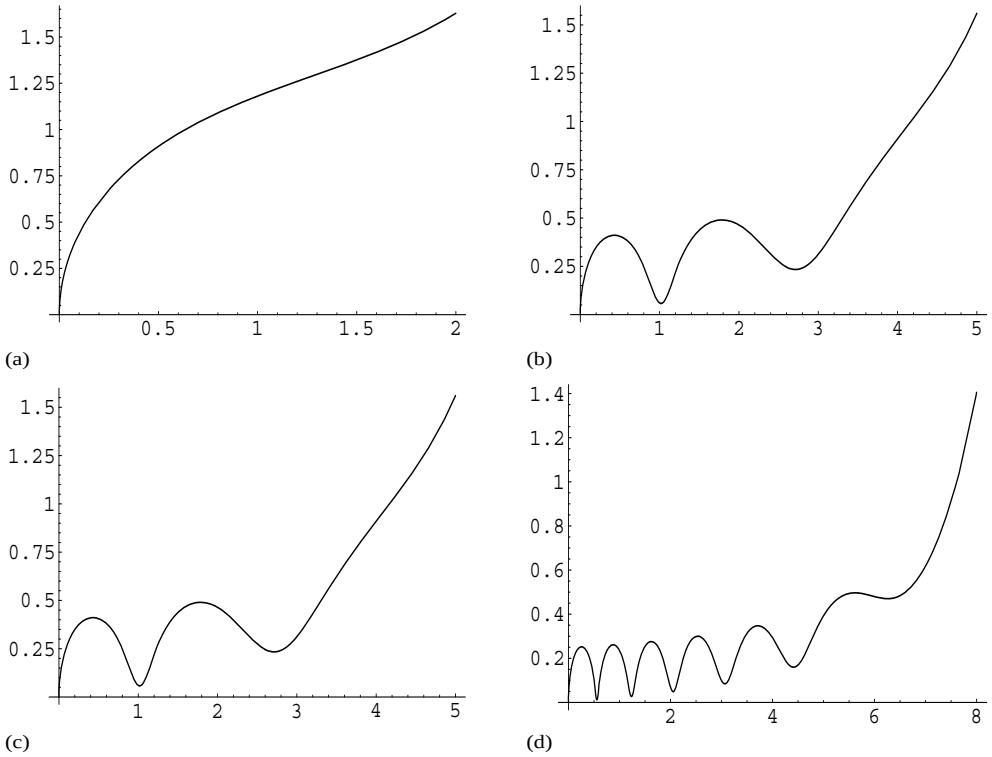

Figure 14: A plot of $y(s)$ against s with (a) $h = 2$, (b) $h = 4$, (c) $h = 5$, (d) $h = 8$.

Solving the ODE numerically in Mathematica with $c = 1/R$ for $R = 2000$, and $h = 2, 4, 5, 8$ (everything in units of L) provides the results shown in Figure 14. This computation suggests that for h of order 10, the solution, which starts as a sphere, blows up before reaching $s = h$. Also the solutions for $h = 4$ and 5 show places where $y'(s) = 0$ (for instance at $s_c \approx 1$). A droplet with this shape cannot be stable, because if the profile is stretched in the s-direction by a small amount near s_c, with consequent thinning there, then the surface tension force across the plane $s = s_c$ will no longer be enough to hold the

region $s < s_c$ against the centrifugal force. A further point to note is that the solution for $h = 2$ does not in fact connect smoothly to a thin layer of liquid on the surface of the cylinder at $s = h$ in the way we supposed. It can in fact be shown that the assumption of this connection ($p_0 = p_a + \gamma/R$ or in dimensionless form $c = 1/R$) is not consistent. Further work along these lines would therefore have to drop that assumption and use values of $c < 1/R$.

References

[1] Applied Partial Differential Equations. J.R. Ockendon, S. Howison, A. Lacey and A. Movchan. Oxford University Press, 1999.

[2] Axisymmetric Fluid-Liquid Interfaces. S. Hartland and S.W. Hartley. Elsevier, 1976.